Changes in the firn structure of the western Greenland Ice Sheet caused by recent warming

S. de la Peña[1], I. M. Howat[2], P. W. Nienow[3], M. R. van den Broeke[4], E. Mosley-Thompson[1], S. F. Price[5], D. Mair[6], B. Noël[4], and A. J. Sole[7].

[1]Byrd Polar and Climate Center, The Ohio State University, Scott Hall, 1090 Carmack Road, Columbus, OH, 43212, USA. santiagodpr@gmail.com

[2]School of Earth Sciences, The Ohio State University, 125 South Oval Mall, Columbus, OH 43210-1002, USA

[3]School of GeoSciences, The University of Edinburgh, Geography Building, Drummond Street, Edinburgh EH8 9XP, UK

[4]Institute for Marine and Atmospheric research Utrecht (IMAU), Utrecht University, P.O. Box 80000, 3508 TA Utrecht, The Netherlands

[5]Fluid Dynamics Group, Los Alamos National Laboratory, T-3, Mail Stop B216, Los Alamos, NM 87545, USA

[6]The College of Physical Sciences, University of Aberdeen, Fraser Noble Building, King's College, Aberdeen, AB24 3UE, UK

[7]Department of Geography, The University of Sheffield, Sheffield, S10 2TN, UK

ABSTRACT. Atmospheric warming over the Greenland Ice Sheet during the last two decades has increased the amount of surface meltwater production, resulting in the migration of melt and percolation regimes to higher altitudes and an increase in the amount of ice content from refrozen meltwater found in the firn above the superimposed ice zone. Here we present field and airborne radar observations of buried ice layers within the near-surface (0-20 m) firn in western Greenland obtained from campaigns between 1998 and 2014. We find a sharp increase in firn-ice content in the form of thick widespread layers in the percolation zone, which decreases the capacity of the firn to store meltwater. The estimated total annual ice content retained in the near-surface firn in areas with positive surface mass balance west of the ice divide in Greenland reached a maximum of 74 ± 25 Gt in 2012, compared to the 1958-1999 average of 13 ± 2 Gt, while the percolation zone area more than doubled between 2003 and 2012. Increased melt and column densification resulted in surface lowering averaging -0.80 ± 0.39 m yr^{-1} between 1800 and 2800 m in the accumulation zone of western Greenland. Since 2007, modeled annual melt and refreezing rates in the percolation zone at elevations below 2100 m surpass the annual snowfall from the previous year, implying that mass gain in the region is retained after melt in the form of refrozen meltwater. If current melt trends over high elevation regions continue, subsequent changes in firn structure will have implications for the hydrology of the ice sheet and related abrupt seasonal densification could become increasingly significant for altimetry-derived ice sheet mass balance estimates.

1. Introduction

Investigations in the percolation zone of the Greenland Ice Sheet (GrIS) have revealed a highly variable snowpack structure characterized by the presence of ice lenses, pipes, and layers (*Benson*, 1962; *Scott et al.*, 2006a; *Parry et al.*, 2007; *Harper et al.*, 2012). The heterogeneous snowpack characteristic of this region results from periods of relatively high snow accumulation followed by short melt events during summer. During melt episodes, surface meltwater percolates through the snowpack and may refreeze at depth. The atmosphere has warmed considerably in the last decade over the GrIS (*van den Broeke et al.*, 2009; *Box et al.*, 2012; *Bennartz et al.*, 2013), with 2010 and 2012 being the warmest years in western Greenland since records began (*Tedesco et al.*, 2011 and 2013; *Bennartz et al.*, 2013; *Tingley and Huybers*, 2013). As a consequence, the area of the ice sheet covered by percolation facies has grown, and the amount of surface melt and subsequently refrozen meltwater retained in the firn has increased (*Tedesco et al.*, 2008; *Fettweis et al.*, 2011; *Harper et al.*, 2012, *Fettweis et al.*, 2013; *van Angelen et al.*, 2014). Extreme warming events such as in July 2012 (*Nghiem et al.*, 2012; *Bennartz et al.*, 2013) have further intensified melt, but it is unknown whether increasing meltwater production and subsequent percolation and refreezing at high elevations has shifted the equilibrium line higher and affected the buffering and transport of meltwater over the interior of the ice sheet. Furthermore, these processes and their high spatial and temporal variability have implications for altimetry-derived mass balance estimates.

A model-based study by *Pfeffer et al.* (1991) showed that predictions of runoff-induced sea level rise from Greenland that did not consider meltwater refreezing within the firn could be overestimating sea level rise by as much as 5 cm over the next 150 years. The importance of meltwater retention was further highlighted by a study (*Harper et al.*, 2012) based on field measurements obtained in 2007, 2008 and 2009 along the Expédition Glaciologique Internationale au Groenland (EGIG) line in western Greenland. *Harper et al.* (2012) estimated that Greenland's firn has the potential to store between 322 and 1289 Gt of meltwater, confirming its importantce as a buffer between surface melt and runoff. Firn-ice content was greater than 50% by volume at altitudes below 1600 m, decreasing steadily with elevation. At the time, the presence of ice at an elevation of 2000 m was found to be relatively uncommon. That work added to a series of studies conducted between 2003

and 2006 as part of the first CryoSat Validation Experiment that helped assess near-surface snowpack and firn conditions at the higher end of the percolation zone (1950-2350 m). The CryoSat validation work focused on the region's spatially variable stratigraphy, as characterized by the presence of thin ice layers that were the main source of backscatter of Ku-band altimeter signals (*Scott et al.*, 2006a; *Parry et al.*, 2007; *Helm et al.*, 2007). Together, these studies can provide a decadal record of ice content and can be linked with earlier data from the National Aeronautics and Space Administration (NASA) Program for Arctic Regional Climate Assessment (PARCA, *Abdalati et al.*, 1998). In the late 1990s, PARCA collected scores of shallow firn and ice cores to quantify spatial and temporal variability of annual accumulation rates over the GrIS (e.g. *McConnell et al.*, 2000; *Bales et al.*, 2001; *Mosley-Thompson et al.*, 2001).

Here, we use snowpit data and airborne radar and laser remote sensing observations from the percolation zone of western Greenland in conjunction with output from regional climate model of melt, runoff, and snow accumulation to a) quantify changes in percolation conditions after the unusually warm years of 2010 and 2012; b) identify areas where widespread ice layers formed by meltwater percolation and refreezing are found; and c) assess the state and extent of the percolation zone of the GrIS given current melt trends over the ice sheet interior. For this, we estimated the total ice content and area covered by percolation facies resulting from melting and refreezing patterns across a wide elevation range on the western slope of the GrIS. Our field sites are all located within one degree of latitude (69.2°N – 71.1°N) on the western slope of the ice sheet, spanning an elevation range from 1900 to 2500 m (Figure 1). At each site, snowpits were excavated in April of 2011, 2012, 2013, and 2014 in order to characterize regional near-surface (~2-3 m) snowpack conditions and percolation facies in the region following the melt season from the previous year. Extensive melt layers were identified and traced using airborne radar to identify areas covered by percolation facies, and airborne laser altimetry data were used to estimate annual elevation changes in the region. Additionally, output from the Regional Atmospheric Climate Model (RACMO2.3/GR, *van Meijgaard et al.*, 2008; *Ettema et al.*, 2009; *van den Broeke*, 2009) are used to assess, at a regional scale, the intensity and extent of the abnormally strong 2010 and 2012 melt seasons in Greenland's accumulation zone that led to the sharp increase in the observed firn-ice content.

2. Methods and Observations

We measured firn ice content by measuring ice layer thickness in snow pits made during April (pre-summer melt) field campaigns between 2011 and 2014. The 2011 campaign was part of CryoSat-2 validation activities continuing efforts initiated in 2004 and 2006 (*Parry et al.*, 2007; *Scott et al.*, 2006a and 2006b; *Helm et al.*, 2007). Near-surface density and stratigraphy measurements were obtained from snow pits at 4 sites in the upper end of the percolation zone, located between 2350 and 2490 m along the EGIG line (named T12-T15 hereafter for historical reasons). The April 2012, 2013 and 2014 campaigns were part of a study of outlet glacier dynamics and also included snow pit surveys of winter accumulation and ice layer thickness at four sites in the catchment of Jakobshavn Glacier (hereafter referred as J1-J4 sites) between elevations of 1935 and 2350 m (Figure 1). Additionally, we extended the firn-ice content record in this area back in time to 1977 using 3 shallow firn cores drilled in 1998 at 2000 m, 2500 m, and 2795 m elevation (69°N 45°W; 69°N 43°W; and 69°N 41°W) as part of PARCA. The cores were dated using a combination of the winter minima in the seasonal variations of dust concentration, $\delta^{18}O$, and H_2O_2 (*Mosley-Thompson et al.*, 2001). Although the thickness of each annual layer (after being converted to water equivalent using density) can be ascertained using any one of these parameters, for this study the layer thicknesses (net accumulation) were calculated using the winter minima in dust concentration.

121   We used remote sensing observations acquired by NASA's Operation IceBridge Snow Radar
122   and the Airborne Topographic Mapper (ATM). The Snow Radar is a wideband radar that operates in
123   the 2-6.5 GHz frequency range and can map polar firn internal layers with a range resolution of ~5
124   cm (*Panzer et al.,* 2013; *Leuschen et al.*, 2014), and is used to trace the ice layers beneath the winter
125   accumulation in 2011 by identifying internal radar reflections caused by melt layers. The ATM is a
126   scanning laser altimeter used in this study to estimate annual elevation change between 2010 and 2013
127   along a frequently repeated transect in western Greenland (Figure 1).

128   Output data from the RACMO2.3/GR model with a horizontal resolution of ~11 km (*Ettema*
129   *et al.*, 2009; *van den Broeke*, 2009) are used in combination with the remote sensing observations to
130   map the percolation zone extent. For the GrIS, RACMO2.3/GR is coupled to a physical multilayer
131   snow model that treats surface albedo as a function of melt as well as percolation and refreezing
132   (*Bougamont et al.*, 2005; *Van Angelen et al.,* 2014). A recent study comparing RACMO2.3/GR results
133   with melt rates derived from the Scanning Multichannel Microwave Radiometer (SMMR) mission
134   shows that discrepancies between the model and satellite data occur mainly in areas of high meltwater
135   runoff (*Fettweis et al.*, 2011), due in part to the lack of remote sensing capability of assessing melt
136   and runoff rates. There is good agreement at higher elevations, which suggests that assumptions about
137   snowpack heat transfer and energy balance in the model are well parameterized for the percolation
138   zone of the GrIS. Thus, the model results used here are limited to regions with no simulated meltwater
139   runoff. The logic for the estimates for total ice content derived from the model results is as follows: at
140   the lower elevations of this no-runoff area where modeled melt exceeds total accumulation, with total
141   firn ice content water equivalent values close to total accumulation. At higher elevations, total firn ice
142   content measured in the field and presented in Section 3 of this paper represents a percentage of the
143   total modeled melt. This percentage of the modeled melt in the form of observed firn-ice decreases
144   with elevation. This is the main cause of the relatively large uncertainty in the estimates of the total
145   refrozen meltwater presented in Section 4.

146   **3. Snowpack Structure**

147   Figure 2a illustrates the ice layers and lenses present in each PARCA core's visible stratigraphy.
148   Cores 6945 and 6943 (named for the coordinates where they were acquired) are ~18 m long and
149   extend back to 1976 while core 6941 is 11.7 m long and extends to a depth equating to 1985's
150   accumulation. The thickness of the different annual layers is affected by annual snowfall, deflation
151   and re-deposition by wind, compaction, and melting, and varies on the order of tens of cm from year
152   to year in western Greenland (*McConnell et al.*, 2000; *de la Peña et al.*, 2010; *Burgess et al.*,
153   2010). Small amounts of ice are commonly found in the core, but are not present on an annual basis.
154   While no ice was observed in core 6945 over the periods of 1977-1979 and 1996-1997, between 1987
155   and 1991 several thin ice layers were found separated by a few cm. Most layers were found to be 3-4
156   cm thick, and the thickest (1989) was 9 cm thick. Cores 6943 and 6941 show similar patterns, with
157   occasional ice layers 1-2 cm thick.

158   Current conditions are represented in the schematic (Figure 2b), made from measurements of
159   winter snow depth and ice layer thickness for each site visited during spring in 2013 and 2014 and
160   illustrating the near-surface stratigraphy as found in spring 2014. Ice content measured in 2011 at
161   T12, a site located at the same altitude as J4 but roughly 10 km north is included as well. The
162   stratigraphy of the shallow firn cores shows that at least between 1977 and 1997, melt events at higher
163   elevations were more rare and much less intensive relative to those observed since. The extreme melt
164   events of 2012 created conditions that facilitated the formation of impermeable ice layers several
165   times thicker than previously observed across this elevation in the percolation zone of the GrIS. These

166 layers were found at all sites visited and appear to be continuous throughout the area surveyed. In
167 2004, total ice thickness at an elevation of 1950 m averaged 10 cm (*Parry et al.*, 2007), significantly
168 less than the ice content in 2013 at J4, located 400 m higher on the ice sheet. The total mass of the ice
169 layers found at the J sites averaged 441 ± 12 kg m^{-2} (0.48 ± 0.013 m thick) and 306 ± 118 kg m^{-2} (0.33
170 ± 0.128 m thick) in 2013 (related to 2012 melt season) and 2014 (related to 2013 melt season)
171 respectively. In April 2011 at the higher elevation sites, the total ice layer mass was 285, 255 and 160
172 kg m^{-2} for T12, T13 and T14 respectively. Ice content decreased at T15 (h = 2490 m), where an ice
173 layer just 4 cm thick (36 kg m^{-2}) was found, suggesting this site was close to the boundary of the dry
174 snow zone that year. At the J-sites, winter accumulation was measured at 1.11 ± 0.17 m, 0.885 ± 0.08
175 m, and 1.35 ± 0.07 m in the winters of 2011-2012, 2012-2013 and 2013-2014 respectively. The 2010-
176 2011 winter accumulation measured at the T12-T15 sites was 1.10 ± 0.12 m. Winter snow density was
177 measured in 2011 and exhibited little variability (247 ± 8 kg m^{-3}), consistent with previous
178 observations (*Parry et al.*, 2007). Total annual ice content found beneath the wintertime snow
179 accumulation during each of the campaigns described in the previous section is summarized in Figure
180 3, revealing the sharp increase in firn-ice content since 2010, where the annual ice layers were an
181 order of magnitude thicker in total than the 1977-1997 average from PARCA core 6945.

182   Measurements in April 2011 by the NASA Snow Radar show the extent of the type of
183 percolation features as described above that formed during the 2010 melt season (Figure 4). Data for
184 the years 2012 and 2013 is not available. The ~420 km-long transect extends from the ablation zone
185 to the ice divide in the dry snow zone and overflights close to our research sites. Radar signals are
186 partially backscattered from within a stratified snowpack by abrupt changes encountered in snow
187 density and/or ice structure, such as ice layers in the percolation zone, or 'autumn hoar' in the dry
188 snow zone. Near surface layering is observed in the 1600-2200 m elevation range and winter
189 accumulation over the previous summer melt layer is clearly resolved while deeper layers are
190 obscured by infiltration ice that limits radar signal penetration. The topmost reflection under the
191 observed winter surface is continuous over most the percolation zone, confirming that ice layers
192 observed at the J field sites are widespread over an elevation range of 1600 to 2200 m, about 220 km
193 inland from the ice margin. The ice layer was retraced with a custom-made threshold algorithm
194 configured to identify strong reflections underneath the surface (shown with a black line in Figure 4).
195 The retracker was applied up to 2450 m, elevation at which isochrones can be observed to a depth
196 greater than 5 m, evidence that no significant amount of ice is present in the snowpack to prevent
197 radar signal penetration. The threshold algorithm tracks continuity between horizontally adjacent
198 pixels, so that the retraced layer in one individual radar acquisition is not separated vertically by more
199 than ~20 cm from the next measurement. In some sections the buried signal could not be
200 differentiated from the surface, and at some points there is discontinuity in the signal. However, for
201 most of the percolation zone the reflection appears continuous, tracked at a depth of 0.81 ± 0.29 m,
202 slightly lower than the field measurements at T sites. The underestimation is likely the result of
203 tracking on the leading edge of the signal and does not affect our analysis.

204   At higher elevations, annual accumulation layers are clearly seen to depths of at least 15 m,
205 consistent with previous observations from the dry snow zone (*Hawley et al.,* 2005; *de la Peña et al.*,
206 2010; *Simonsen et al.*, 2013). While melt has intensified over the last decade, the 2012 melt episodes
207 had notably bigger impacts on the firn structure, with significant melting and infiltration extending to
208 the ice divide (*Tedesco et al.*, 2013). Figure 5 shows annual elevation changes over the same transect
209 shown in Figure 4 obtained from repeat ATM lidar overflights between 2010 and 2013. While snow
210 accumulation variability and ice dynamics are factors in the observed surface elevation change,
211 lowering of the magnitude observed in 2012-2013 must be the result of surface melt, infiltration and

densification of the firn, since variability in annual snow accumulation is not large enough to cause the departure seen in 2012-2013, and there is no indication that dynamic thinning during that year was significantly different from previous years. Average elevation change estimated across the 1600-2600 m elevation range is -0.803 ± 0.391 m yr^{-1}, compared to -0.112 ± 0.067 m yr^{-1} and 0.031 ± 0.188 m yr^{-1} in 2010-2011 and 2011-2012 respectively. This difference does not represent a loss in mass but rather a rapid densification of the near-surface structure of the firn, with surface lowering observed almost to the ice divide.

4. Melt intensity and extent of the percolation zone

Figure 6 presents results from RACMO2.3/GR between 1958 and 2013 for each of the sites visited between 2011 and 2014, and Table 1 shows modeled melt and accumulation rates for the years 2003, 2010, and 2012. Melt at J1 increased from 340 kg m^{-2} in 2003 to 810 kg m^{-2} in 2012 (3 times the 1958-1999 average of 285 kg m^{-2}), but as discussed in the previous section, total ice content increased more than 5 times over the same period. Ice layer thickness does not increase as a simple function of surface melt. Infiltration of meltwater into firn is complicated by factors including the initial thermal state and structure of the firn and the timing and duration of melt. For example, more frequent extreme melt events, such as the event that occurred in 2012, may cause rapid snow saturation and refreezing near the surface, resulting in the formation of thicker and more extensive ice layers. The formation of ice reservoirs of this magnitude is thus not only dependent on melt increase, but also on how melt is distributed during summer. Uncertainties in melt and refreezing rates in RACMO2.3/GR add to this complexity, and as a result, it is difficult to confidently predict firn changes using only the model results. For instance, in 2003, the ice layers observed to have formed during the summer at 2000 m elevation accounted for 29% of total modeled melt, while in 2012 discernible ice content was 79% of the modeled melt (52% at the highest site at 2350 m). The 2012 melt season anomaly was driven partly by extreme, short-lived melt episodes (i.e. *Nghiem et al.*, 2012; *Bennartz et al.*, 2013; *Tedesco et al.*, 2013), which as discussed may result in more ice content. Increases in modeled melt rates at higher sites are even more pronounced than at J1, with rates at J4 increasing from less than 100 kg m^{-2} over the period from 1958 to 1999, to a rate of 305 and 580 kg m^{-2} in 2010 and 2012 respectively (Figure 6). Prior to 2012, the largest modeled melt rates occurred in 2010 at all sites except at the highest regions (above 2200 m), which registered the largest melt rate in 2007 (second highest for the lower sites). Large modeled melt rates at all sites occurred during the warm years of 1995, 1998, 2007, and 2010. Melt at J1 increased from less than 300 kg m^{-2} between 1958 and 1999, to 340 kg m^{-2} in 2003 and to 755 kg m^{-2} in 2010. At J4 there was only an increase of 30% in 2010 with respect to 2003 (from 235 to 305 kg m^{-2}), but this increased to 580 kg m^{-2} in 2012. Before 2012, the modeled melt rate at this site was highest in 2007, in contrast to the 2010 peak melt rates estimated for most of the western Greenland margin (*Tedesco et al.*, 2011). The mass of ice found in 2013 at sites J1 and J2 exceeds the mass of the total annual accumulation for 2012, a trend that according to RACMO2.3/GR has been occurring at J1 since 2007. Modeled melt rates in 2013 are significantly lower than in 2012, but still larger than the 1958-1999 average. We found no evidence of meltwater pathways or pond formation at our field sites. If, however, conditions impermeable ice layers keep forming over extensive areas and melt continues to exceed total accumulation, it is likely that lateral supraglacial transport and eventual runoff of excess meltwater will reach to 2000 m elevation in western Greenland.

Figure 7 presents annual melt predicted by RACMO2.3/GR in areas of the GrIS with predicted positive surface mass balance (i.e. the accumulation zone) for each time period presented. The left figure shows the 1958-1999 average, while the right figure is the annual melt rates in 2012, illustrating the changes in melt intensity and the size of the areas affected by melt over Greenland.

258   The predicted average area of the accumulation zone that experienced melt between 1958 and 1999
259   was about 405,000 km^2. The extent of this area then increased 240% in 10 years, from 465,000 km^2 in
260   2003 to a maximum of 1,155,000 km^2 in 2012, more than half the total area of the ice sheet. Although
261   in 2010 the percolation zone covered a total area of 486,000 km^2, only a 5% increase with respect to
262   2003, the intensity of melt increased drastically after 1999, especially in west and southwest
263   Greenland. To quantify the magnitude of refrozen meltwater in 2012, we estimate total annual ice
264   content in western Greenland by identifying areas where snowfall and melt rates are sufficiently high
265   (greater than 100 kg/m^2 per year) to form the stratified snowpack structure described above. We
266   estimate the total mass refrozen in the snowpack in western Greenland by relating melt rates from
267   RACMO2.3/GR to the measured ice content found during 2011 and 2013, and subtract the mass of
268   the snow that occupied the volume where meltwater refroze (total ice content cannot exceed the total
269   winter accumulation). Based on the field measurements, we assume an average winter snow density
270   of 250 kg m^{-3}. Our estimates indicate that the total 2012 infiltration ice content above the equilibrium
271   line and west of the ice divide of the GrIS was 74 ± 25 Gt, compared to an average of only 13 ± 2 Gt
272   between 1958 and 1999. Most of this ice is distributed near the surface solely in the form of thick
273   layers that appear to be widespread.

274   **5. Discussion and conclusions**

275   Our field observations reveal substantial, recent changes in the structure of high-elevation percolation
276   facies that differ from those recorded in previous decades. Observations in 2004 and 2006 showed an
277   increase from the 1977-1997 average ice content, but the lack of significant ice above 2000 m was
278   evidence that the transition between the percolation and dry snow zones was near this elevation (*Scott*
279   *et al.*, 2006b). In contrast, the Snow Radar data obtained in spring 2011 reveals that the percolation
280   zone has risen with the transition in the previous few years occurring at elevations between 2200 and
281   2400 m. More importantly, the concentration of ice at higher elevations has increased dramatically,
282   and the formation of thick, widespread continuous ice layers is increasingly common over extensive
283   areas of the percolation zone causing large changes in the air content of the firn. Furthermore, the
284   increase in firn ice content raises questions regarding the permeability of the firn column across the
285   percolation zone, and the effects it could have on meltwater retention and transport and on firn
286   compaction rates.

287   The formation of percolation facies in the last few decades of the 20th Century above 2000 m
288   was limited, and during some years melt was not even strong enough to form identifiable ice layers. In
289   this context, the percolation features described here have no recent precedent. Considering, as
290   measured in the field, an average surface snow density before melt of 250 kg m^{-3}, and that meltwater
291   refreezes in a volume occupied by snow of this density, each meter of winter snow would equate to
292   layers of ice totaling ~0.35 m thick after refreezing if little or no air remains trapped within. This
293   process will create the observed seasonal change in the volume of the firn governed by accumulation,
294   compaction, and melting and refreezing. Even without thermal snow densification, commonly used
295   steady-state snow density and firn compaction assumptions used for altimetry-derived mass balance
296   estimates would need to be reconsidered for regions where percolation features become more
297   impermeable. These ice layers not only significantly limit the total meltwater buffering capacity of the
298   percolation zone estimated by *Harper et al.* (2012), but also introduce variability in compaction rates
299   if air is trapped within ice layers. Moreover, and as observed at sites J1 and J2, the winter snow in
300   these regions of the accumulation zone of the ice sheet completely melted and refroze in 2012,
301   meaning mass gain in these areas was in the form of superimposed ice. Although the melt season of
302   2012 was unusually warm, rather than an isolated episode it represent the most dramatic example of
303   changes that are occurring due to the above-average warming in western Greenland observed in the

304   last decade.

305   Melt affecting the GrIS has increased over recent decades, with pronounced departures from
306   the 1958-1999 mean melt rate during the last few years in regions well within the accumulation zone
307   of the GrIS. High (and highly variable) accumulation rates play an important role in the surface mass
308   balance of the ice sheet at higher elevations, but with melt rates increasing faster than snow
309   accumulation in Greenland (*Fettweis*, 2007; *Van Angelen et al.*, 2014), meltwater excess during warm
310   years may saturate the already limited firn meltwater storage capacity over large areas (*Van Angelen*
311   *et al.*, 2013). Although no evidence of extensive lateral hydrological pathways was found at any of
312   our field sites, it is likely that if melt continues to exceed total accumulation, water will soon be
313   transported to lower elevations by supraglacial flow, especially during years experiencing extreme
314   melt. Recent studies show that lakes are increasingly found at higher elevations (*Banwell et al.*, 2012;
315   *Liang et al.*, 2012; *Howat et al.*, 2013), and it is unclear how the percolation zone will evolve if more
316   meltwater ponds are being formed over firn. Furthermore, according to RACMO2.3, if current
317   warming trends continue, the percolation zone will potentially extend to most areas above the
318   equilibrium line. Regardless of the role they will play in the future, these huge ice reservoirs are the
319   result of an intense melting process of the same order of magnitude as the total mass imbalance of the
320   GrIS, and the consequences of their formation described here underlines the importance of monitoring
321   the evolution of Greenland's firn layer in the coming years.

322 **Bibliography**

323 Abdalati, W., R. Bales, and R. Thomas (1998). Program for Arctic Regional Climate Assessment. An
324 improved understanding of the Greenland ice sheet. *Arct. Res.*, **12**, 38-54.

325 Bales, R.C., J.R. McConnell, E. Mosley-Thompson, and B. Csatho (2001). Accumulation over the
326 Greenland Ice Sheet from historical and recent records. *J. Geophys. Res.*, **106**(D24), 33, 813-33, 825,
327 doi:10.1029/2001JD900153.

328 Banwell, A.F., Arnold, N.S., Willis, I.C., Tedesco, M., and Ahlstrøm, A.P. (2012). Modeling
329 supraglacial water routing and lake filling on the Greenland Ice Sheet, JGR-Earth Surface, 117,
330 F04012, doi:10.1029/2012JF002393.
331
332 Bell et al., (2008). Spatial and temporal variability in the snowpack of a High Arctic ice cap:
333 Implications for mass-change measurements, *Ann. Glaciol.*, 48, 159–170.

334 Bennartz, R., M.D. Shupe, D.D. Turner, V.P. Walden, K. Steffen, C.J. Cox, M.S. Kulie, N.B. Miller,
335 and C. Pettersen (2013). July 2012 Greenland melt extent enhanced by low-level liquid clouds.
336 *Nature,* 496, 83-86, doi:10.1038/nature12002.

337 Benson, C. (1962). Stratigraphic studies of the snow and firn of the Greenland ice sheet. *Res. Rep.* **70**,
338 U.S. Army Snow Ice and Permafrost Res. Estab.

339 Bougamont, M., Bamber, J. L., and Greuell, W.: A surface mass balance model for the Greenland Ice
340 Sheet, J. Geophys. Res., 110, F04018, doi:10.1029/2005JF000348, 2005.
341
342 Box, J. E., Fettweis, X., Stroeve, J. C., Tedesco, M., Hall, D. K., and Steffen, K.: Greenland ice sheet
343 albedo feedback: thermodynamics and atmospheric drivers, The Cryosphere, 6, 821-839,
344 doi:10.5194/tc-6-821-2012, 2012.
345
346 Burgess, E. W., Forster, R. R., Box, J. E., Mosley-Thompson, E., Bromwich, D. H., Bales, R. C., and
347 Smith, L. C.: A spatially calibrated model of annual accumulation rate on the Greenland ice sheet
348 annual (1958–2007), *J. Geophys. Res.*, 115, F02004, doi:10.1029/2009JF001293.2009, 2010.
349
350 De la Peña, S., Nienow, P., Shepherd, A., Helm, V., Mair, D., Hanna, E., Huybrechts, P., Guo, Q.,
351 Cullen, R., and Wingham, D. (2010). Spatially extensive estimates of annual accumulation in the dry
352 snow zone of the Greenland Ice Sheet determined from radar altimetry, *The Cryosphere*, **4**, 467-474,
353 doi:10.5194/tc-4-467-2010.

354 Ettema, J., M.R. van den Broeke, E. van Meijgaard, W.J. van de Berg, J.L. Bamber, J.E. Box, and
355 R.C. Bales (2009). Higher surface mass balance of the Greenland ice sheet revealed by high-
356 resolution climate modeling, *Geophys. Res. Lett.*, 36, L12501, doi:10.1029/2009GL038110.
357
358 Fettweis, X., M. Tedesco, M. van den Broeke, and J. Ettema (2011). Melting trends over the
359 Greenland ice sheet (1958-2009) from spaceborne microwave data and regional climate models. *The
360 Cryosphere*, **5**, 359-375.

361 Fettweis, X., E. Hanna, C. Lang, A. Belleflamme, M. Erpicum, and H. Gallée (2013). Brief
362 Communication "Important role of the mid-tropospheric atmospheric circulation on the recent surface
363 melt increase over the Greenland ice sheet", *The Cryosphere*, **7**, 241-248, doi:10.5194/tc-7-241-2013.

364 Harper, J., N. Humphrey, W.T. Pfeffer, J. Brown, and X. Fettweis (2012). Greenland ice-sheet

contribution to sea-level rise buffered by meltwater storage in firn. *Nature*, doi:1038/nature11566.

Hawley, R.L., E.M. Morris, R. Cullen, U. Nixdorf, A. Shepherd, and D.J. Wingham (2006). ASIRAS airborne radar resolves internal annual layers in the dry-snow of Greenland", *Geophys. Res. Lett.* **33**(4), L04502, doi:10.1029/2005GL025147.

Helm, V., W. Rack, R. Cullen, P. Nienow, D. Mair, V. Parry, and D.J. Wingham (2007). Winter accumulation in the percolation zone of Greenland measured by airborne radar altimeter. *Geophys. Res. Lett.*, **34**, L06501, doi:10.1029/2006GL029185.

Howat, I.M., de la Peña, S., van Angelen, J.H., Lenaerts, J.T.M., and van den Broeke, M.R. (2013). *Brief Communication* "Expansion of meltwater lakes on the Greenland Ice Sheet", *The Cryosphere*, 7, 201-204, doi:10.5194/tc-7-201-2013.

Leuschen, C., P. Gogineni, R. Hale, J. Paden, F. Rodríguez, B. Panzer, and D. Gomez (2014). IceBridge Snow Radar L1B geolocated radar echo strength profiles, version 2 [20110419, 20130405]. Boulder, Colorado USA: NASA DAAC at the National Snow and Ice Data Center.

McConnell, J.R., Mosley-Thompson, E., Bromwich, D.H., Bales, R.C., and Kyne, J.D. (2000). Interannual variations of snow accumulation on the Greenland Ice Sheet (1985-1996): new observations versus model predictions. *JGR*, **105**, D3, 4039-4046.

Morris et al., (2014). Field-calibrated model of melt, refreezing, and runoff for polar ice caps: Application to Devon Ice Cap. *JGR*, 10.1002/2014JF003100.

Mosley-Thompson, E., J.R. McConnell, R.C. Bales, Z. Li, P.N. Lin, K. Steffen, L.G. Thompson, R. Edwards, and D. Bathke (2001). Local to regional-scale variability of annual net accumulation on the Greenland Ice Sheet from PARCA cores. *J. Geophys. Res.*, **106**(D24), 33, 839-33, 851, doi:10.1029/2001JD900067.

Nghiem, S.V., D.K. Hall, T.L. Mote, M. Tedesco, M.R. Albert, K. Keegan, C.A. Shuman, N.E. DiGirolamo, and G. Neumann (2012). The extreme melt across the Greenland ice sheet in 2012. *Geophys. Res. Lett.*, **39**, L20502, doi:10.1029/2012GL053611.

Parry, V., P. Nienow, D. Mair, J. Scott, B. Hubbard, K. Steffen, D. Wingham (2007). Investigations of meltwater refreezing and density variations in the snowpack and firn within the percolation zone of the Greenland ice sheet. *Annals of Glac.,* 46, 61-68.

Pfeffer, W.T., M.F. Meier, and T.H. Illangasekare (1991). Retention of Greenland Runoff by Refreezing: Implications for Projected Future Sea Level Change. *J. Geophys. Res.*, **96**(C12), 22,117-22,124.

Scott, J., D. Mair, P. Nienow, V. Parry, and E. Morris (2006a). A ground-based radar backscatter investigation in the percolation zone of the Greenland Ice Sheet. *Remote Sens. Environ.*, **104**(4), 361-373.

Scott, J., P. Nienow, D. Mair, V. Parry, E. Morris, and D.J. Wingham (2006b). Importance of seasonal and annual layers in controlling backscatter to radar altimeters across the percolation zone of an ice sheet. *Geophys. Res. Lett.*, **33**, L24502, doi:10.1029/2006GL027974.

Simonsen, S.B., L. Stenseng, G. Adalgeirsdottir, R.S. Fausto, C.S. Hvidberg, P. Lucas-Picher (2013). Assessing a multilayered dynamic firn-compaction model for Greenland with ASIRAS radar

404   measurements. *J. Glac.*, **59**, 215, doi:10.3189/2013JoG12J158.

405   Tedesco, M., M. Serreze, and X. Fettweis (2008). Diagnosing the extreme surface melt event over
406   southwestern Greenland in 2007. *The Cryosphere*, **2**, 159-166, doi:10.5194/tc-2-159-2008.

407   Tedesco, M., X. Fettweis, M.R. Van den Broeke, R.S.W. Van de Wal, C.J.P.P. Smeets, W.J. Van de
408   Berg, M.C. Serreze, and J.E. Box (2011). The role of albedo and accumulation in the 2010 melting
409   record in Greenland. *Environ. Res. Lett.*, **6**, 014005.

410   Tedesco, M., X. Fettweis, T. Mote, J. Wahr, P. Alexander, J.E. Box, and B. Wouters (2013). Evidence
411   and analysis of 2012 Greenland records from spaceborne observations, a regional climate model and
412   reanalysis data. *The Cryosphere*, **7**, 615-630, doi:10.5194/tc-7-615-2013.

413   Tingley, M.P., and P. Huybers (2013). Recent temperature extremes at high northern latitudes
414   unprecedented in the past 600 years. *Nature,* **496**, 201-205, doi:10.1038/nature11969.
415
416   Van den Broeke, M., P. Smeets, J. Ettema, C. van der Veen, R. van de Wal, and J. Oerlemans (2008).
417   Partitioning of melt energy and meltwater fluxes in the ablation zone of the west Greenland ice sheet.
418   *The Cryosphere*, **2**, 179-189.

419   Van den Broeke, M., J. Bamber, J. Ettema, E. Rignot, E. Schrama, W.J. Van de Berg, E. van
420   Meijgaard, I. Velicogna, and B. Wouters (2009). Partitioning Recent Greenland Mass Loss. *Science*,
421   326, 984-986, doi:10.1126/science.1178176.

422   Van Meijgaard, E., L. H. van Ulkft, W. J. van de Berg, F. C. Bosveld, B. J. J. M. van den Hurí, g.
423   Lenderink, and A. P. Siebesma (2008). The KNMI regional atmospheric climate model, version 2.1,
424   *KNMI Tech. Rep*. 302, R. Neth. Meteorol. Inst., De Bilt, Netherlands.

425   Van Angelen, J. H., J. T. M. Lenaerts, M. R. van den Broeke, X. Fettweis, and E. van Meijgaard,
426   (2013). Rapid loss of firn pore space accelerates 21st century Greenland mass loss, *Geophysical*
427   *Research Letters* **40**, doi:10.1002/grl.50490.
428
429   Van Angelen, J. H., M. R. van den Broeke, B. Wouters and J. T. M. Lenaerts, (2014). Contemporary
430   (1960–2012) evolution of the climate and surface mass balance of the Greenland ice sheet, *Surveys of*
431   *Geophysics*, doi: 10.1007/s10712-013-9261-z.

| Site	Latitude	Longitude	Elevation (m)	Melt (kg/m^2) 2003/2010/2012	Accumulation (kg/m^2) 2003/2010/2012
J1	69.212˚ N	46.152˚ W	1935	340 / 753 / 808	520 / 497 / 648
J2	69218˚ N	45.566˚ W	2090	250 / 569/ 729	513 / 644 / 500
J3	69.221˚ N	44.762˚ W	2245	87/ 341 / 637	505 / 492 / 635
J4	69.221˚ N	44.089˚ W	2350	31 / 305/ 580	505 / 480 / 628
T12	70.175˚ N	45.345˚ W	2345	37 / 195/ 502	498 / 548 / 599
T13	70.274˚ N	45.008˚ W	2455	17/ 178 / 507	501 / 550 / 604
T14	70.302˚ N	44.757˚ W	2464	17 / 170 / 455	496 / 546 / 601
T15	70.302˚ N	44.574˚ W	2490	13 / 104 / 399	493 / 538 / 601

432   **Table 1:** Melt and accumulation at each field site as simulated by RACMO2.3/GR.

433
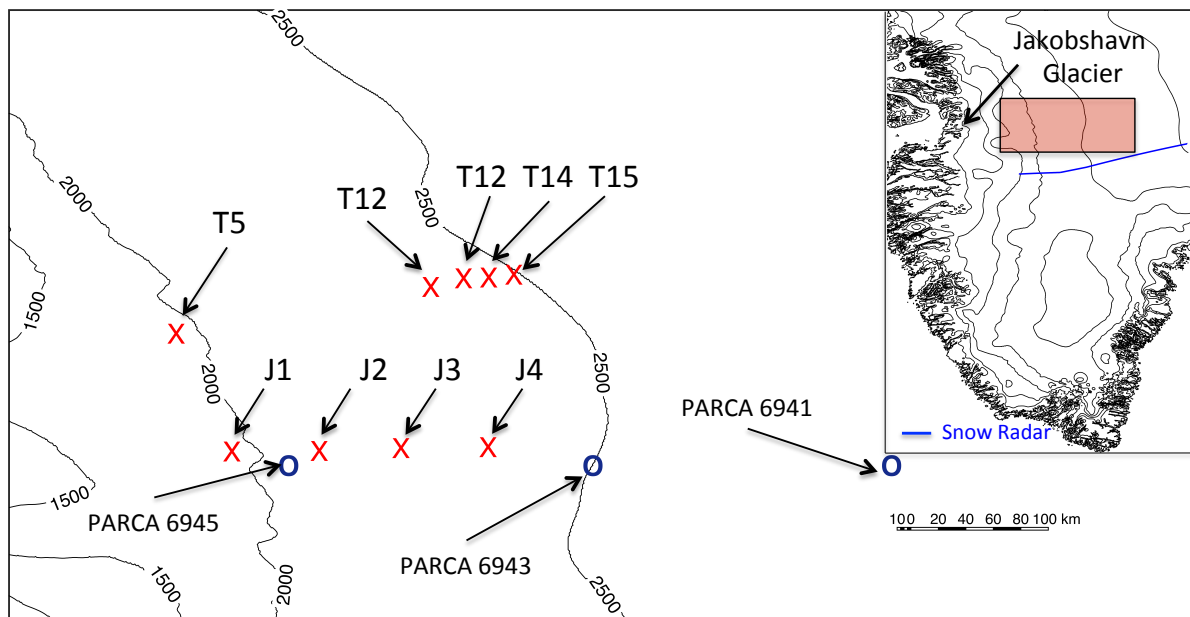
Figure 1. Location of research area and research sites (all T-sites are along the EGIG line). Inset: map of western Grenland showing the area surveyed. Blue line is the flightpath of the NASA Operation IceBridge data shown in Figure 4 and 5. Snowpit sites are shown with an X, while core sites are shown with a blue circle. Contour lines represent 500 m surface elevation intervals.
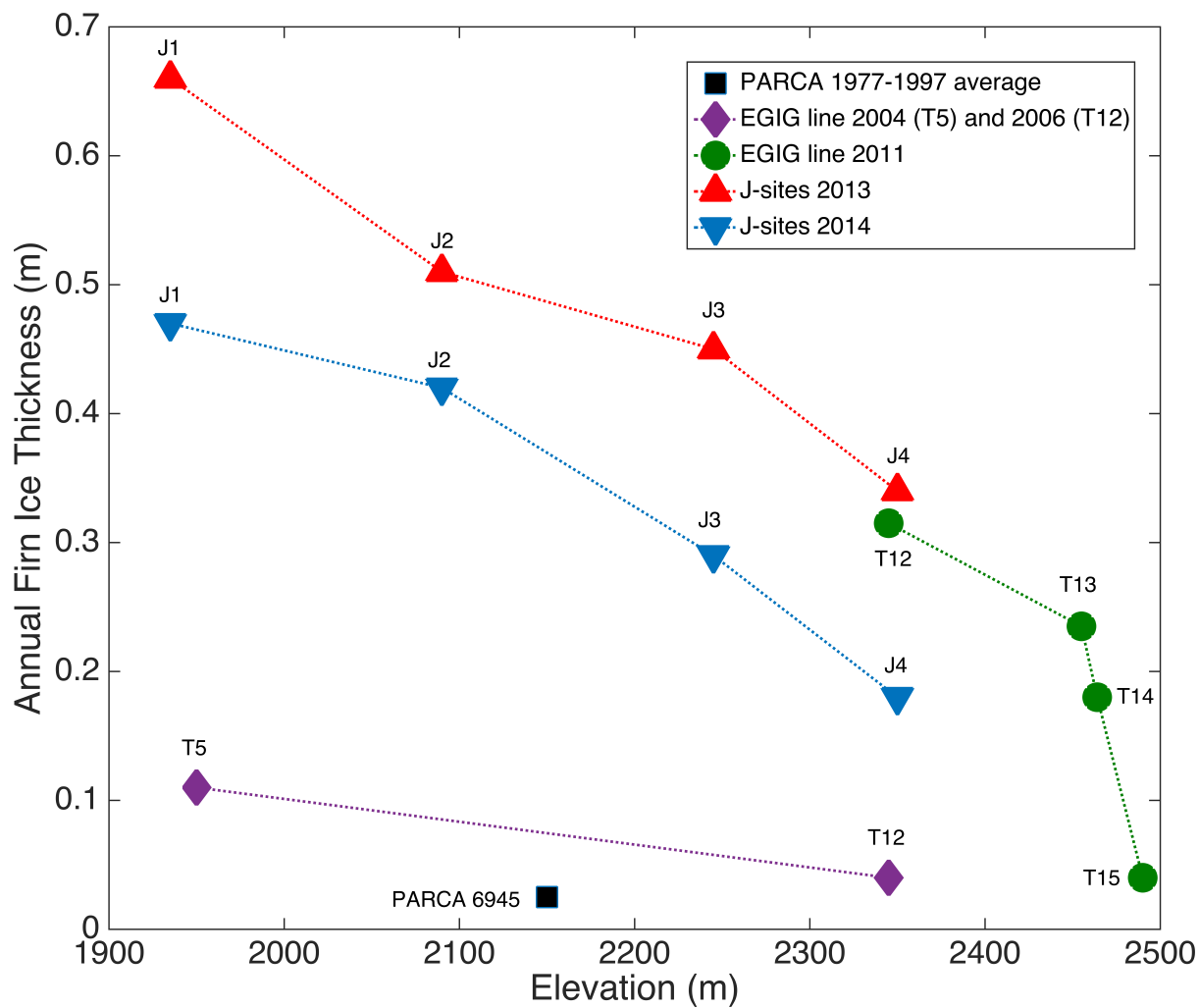
Figure 2. Firn ice content vs. elevation measured in field campaigns between 1998 and 2014. All measurements taken from snow pits except PARCA 1977-1997 average, taken from core 6945.
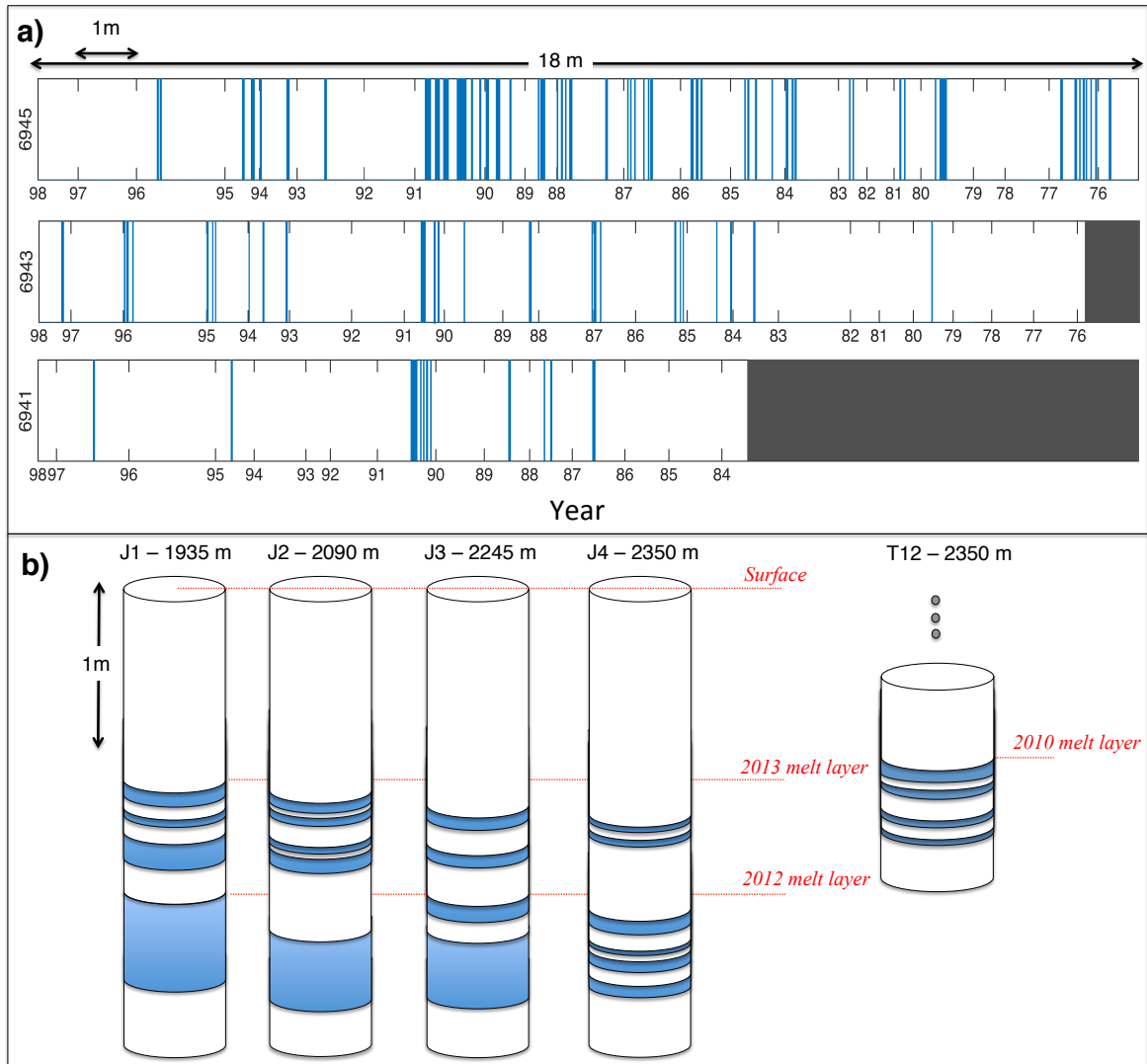
Figure 3. a) Ice layers and ice lenses present in the visible stratigraphy of PARCA firn cores 6941, 6943, and 6945 drilled in 1998 are plotted with depth in core (m). The deepest core is 18 m long and the dates are assigned at the depth (m) of each year's winter minima in dust concentration. b) Schematic showing ice layer structure as measured in snow pits excavated between 2011 and 2014. The melt layer dashed lines indicate the position where the top of the ice layer was found in the field at J1 for the J-sites, and at T12. J-sites are represented as found in April 2014. T12 representation is shown as found in 2011.
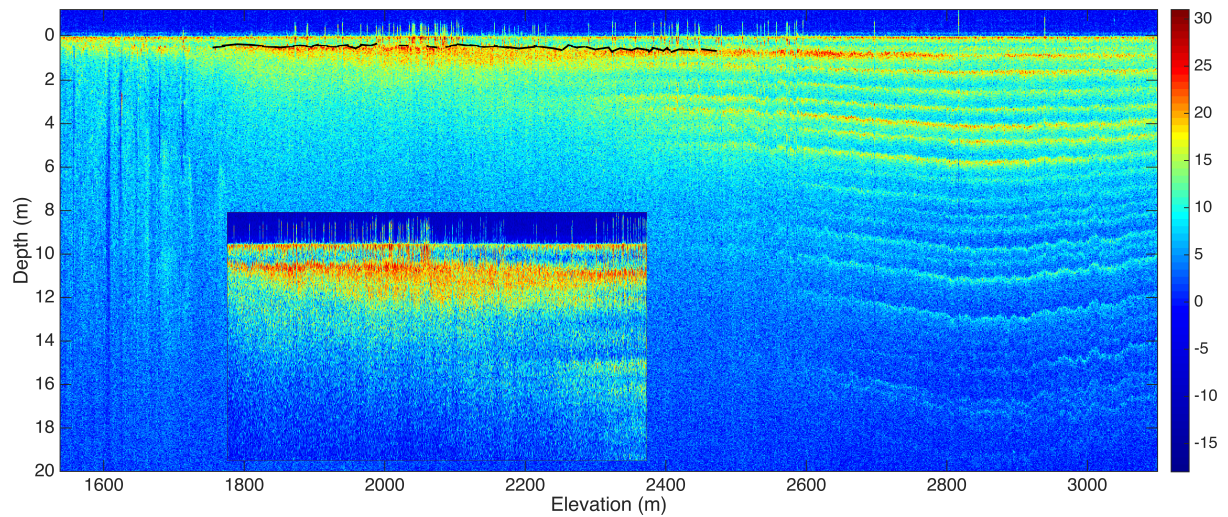
Figure 4. A transect in western Greenland showing Operation IceBridge Snow Radar response to the snowpack in 2011. The aerial survey extends (left to right) from the ablation zone to the dry snow zone. The color scale shows the relative power intensity (in dB). The black line shows the position where the melt layer (i.e. the top of the ice layer formed after the 2010 melt season) was retraced. Inset shows the upper ~5 meters where the melt layer is located.
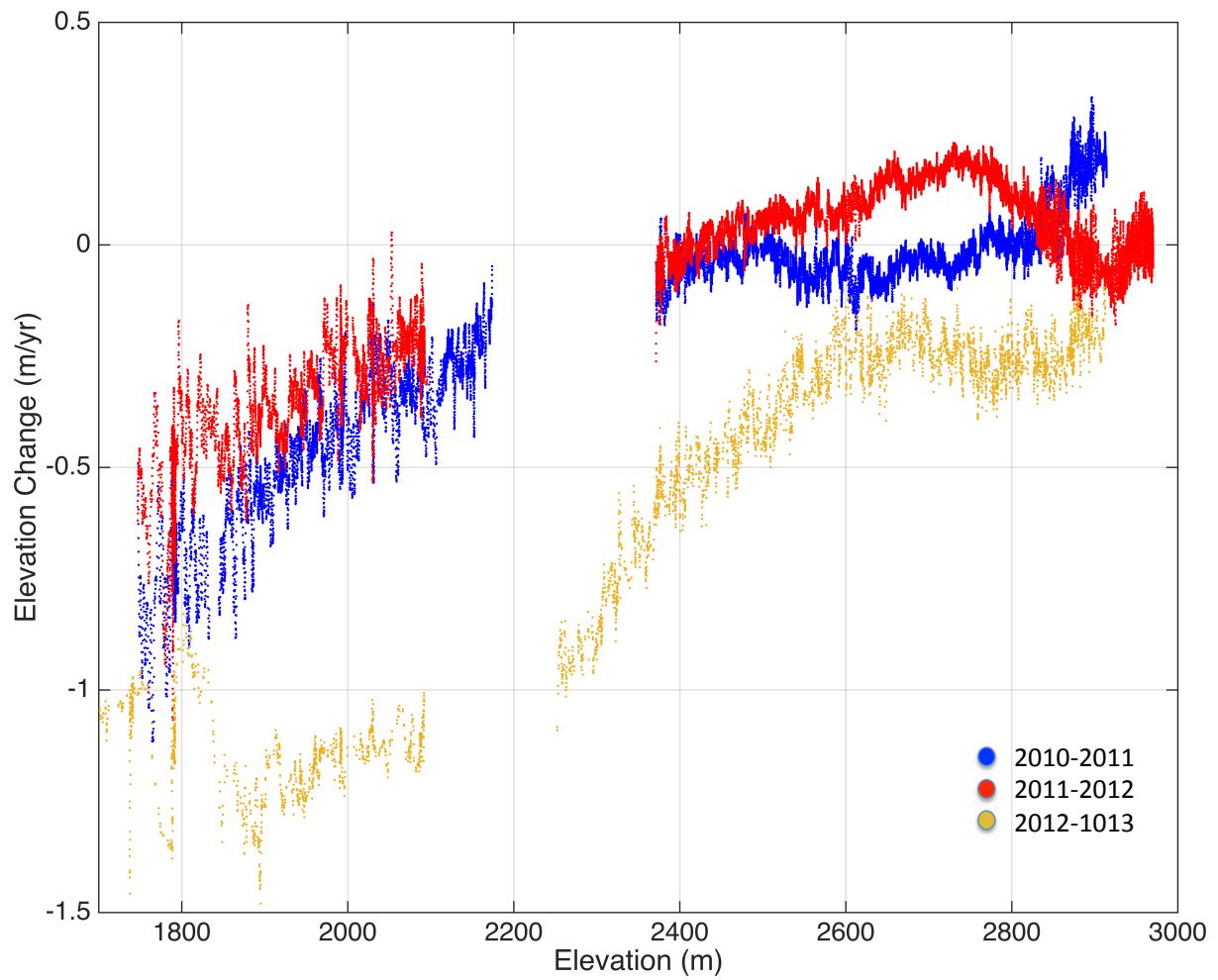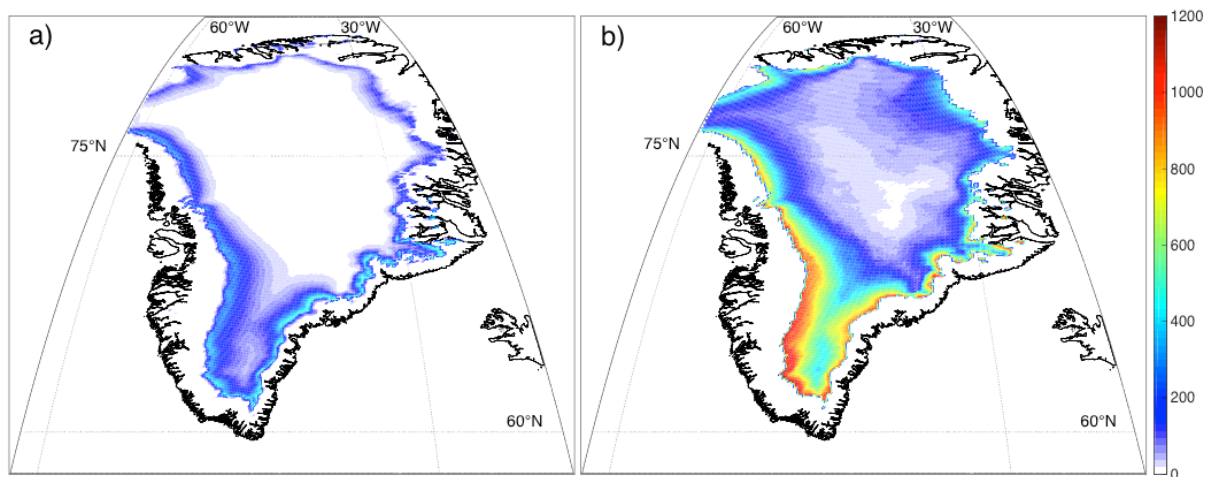
Figure 5. Elevation change estimated from NASA ATM laser altimeter in western Greenland along the flight path shown in Figure 1. Estimates are for annual change in 2011 (blue), 2012 (red), and 2013 (yellow).

460
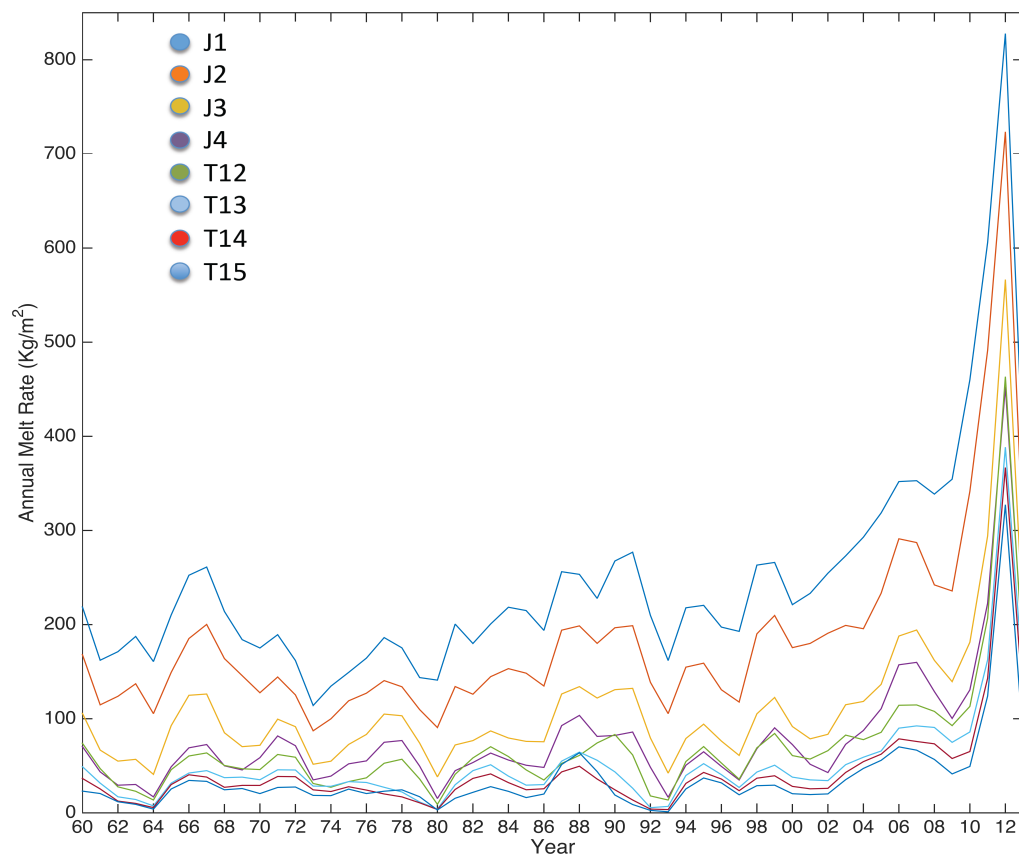
461 **Figure 6.** 1958-2013 Modeled annual melt rates from RACMO2.3/GR for each field site visited
462 between 2011 and 2014.

Figure 7. Regional Atmospheric Climate Model (RACMO2.3/GR) annual melt rates (kg m^{-2}) shown for areas of the GrIS with predicted positive surface mass balance (i.e. above the equilibrium line). Annual melt rates shown for a) the 1958-1999 average and b) for 2012.